

## Article

# Insulation Condition Assessment in Inverter-Fed Motors Using the High-Frequency Common Mode Current: A Case Study

Mariam Saeed , Daniel Fernández , Juan Manuel Guerrero , Ignacio Díaz  and Fernando Briz \* 

Department of Electrical, Computer & System Engineering, University of Oviedo, 33204 Gijón, Spain; saeedmaria@uniovi.es (M.S.); fernandezalodaniel@uniovi.es (D.F.); guerrero@uniovi.es (J.M.G.); idiaz@uniovi.es (I.D.)

\* Correspondence: fbriz@uniovi.es

**Abstract:** The use of the common mode current for stator winding insulation condition assessment has been extensively studied. Two main approaches have been followed. The first models the electric behavior of ground-wall insulation as an equivalent RC circuit; these methods have been successfully applied to high-voltage high-power machines. The second uses the high frequency of the common mode current which results from the voltage pulses applied by the inverter. This approach has mainly been studied for the case of low-voltage, inverter-fed machines, and has not yet reached the level of maturity of the first. One fact noticed after a literature review is that in most cases, the faults being detected were induced by connecting external elements between winding and stator magnetic core. This paper presents a case study on the use of the high-frequency common mode current to monitor the stator insulation condition. Insulation degradation occurred progressively with the machine operating normally; no exogenous elements were added. Signal processing able to detect the degradation at early stages will be discussed.

**Keywords:** high-frequency common mode current; inverter-fed motors; insulation monitoring



**Citation:** Saeed, M.; Fernández, D.; Guerrero, J.M.; Díaz, I.; Briz, F. Insulation Condition Assessment in Inverter-Fed Motors Using the High-Frequency Common Mode Current: A Case Study. *Energies* **2024**, *17*, 470. <https://doi.org/10.3390/en17020470>

Academic Editors: Moussa Boukhniher and Larbi Djilali

Received: 12 December 2023

Revised: 12 January 2024

Accepted: 15 January 2024

Published: 18 January 2024



**Copyright:** © 2024 by the authors. Licensee MDPI, Basel, Switzerland. This article is an open access article distributed under the terms and conditions of the Creative Commons Attribution (CC BY) license (<https://creativecommons.org/licenses/by/4.0/>).

## 1. Introduction

Variable speed drives are commonly used in multiple fields such as transportation, wind power, and industrial machinery, requiring high reliability. Stator insulation failure has been reported as the second most frequently occurring fault in induction machines [1–3]. The exposition of the machine windings to high rates of voltage change ( $dv/dt$ ) due to switches commutation has been early reported to have adverse effects on the insulation [4], which are worsened with the use of new fast switching wide-bandgap devices [5–9].

The better-established insulation monitoring methods are offline, most of them being specific for high-voltage machines [2,3,10,11]. These include insulation resistance, high potential, capacitance, dissipation factor, and partial discharge among others. A main drawback is that the machine has to be removed from service; also, some of these tests are invasive.

A number of methods have also been proposed for insulation monitoring of inverter-fed low-voltage machines. Especially appealing are methods that use the phase current as a vast majority of modern drives include current sensors for control and protection purposes. These methods are often referred to as *Motor Current Signature Analysis* (MCSA) [12–16], but noting that many forms of signal processing are possible [17,18]. A concern with these methods is their capability to detect insulation faults at an early stage. Current sensors are selected according to the control needs, and might not comply with the bandwidth and sensitivity requirements to detect incipient faults. It is noted in this regard that for the experimental verification, it is a common practice to add external resistors to the test machine to emulate the fault [13–15,17–19]; there is no evidence that these kinds of artificial faults will produce similar effects to those due to the actual insulation degradation.

The use of the common mode current has been explored as a means to detect insulation degradation at early stages. While the method is well established for high-voltage, line-connected machines [2,3,20–22], its application to low-voltage, inverter-fed machines are less mature [7–10,23–29].

This paper presents a case study on the use of the high-frequency common mode current to monitor the stator insulation condition. Although this paper will focus on the case of an induction machine, the conclusions might be extended to other types of AC machines with similar stator designs as permanent magnet and synchronous reluctance machines. Aging was accelerated by performing a sequence of experiments in which the machine was forced to operate at temperatures above its insulation class. Insulation degradation occurred progressively, and without adding exogenous elements. Methods for the signal processing capable of detecting the degradation at early stages will be discussed.

The main contributions of the presented paper are: (1) insulation degradation is performed progressively, without artificially provoking the fault and without any exogenous elements (e.g., external resistors or capacitors) following, therefore, a process closer to that occurring in real-world conditions; (2) it has been confirmed that the high-frequency behavior of the zero sequence current is sensitive to insulation degradation even at incipient stages (when the DC insulation resistance is still very high); (3) it has been shown that the behavior of the zero sequence current during the degradation process differs significantly from the behavior observed using artificially induced faults; (4) consequently, it has been shown that signal processing methods and metrics developed based on results obtained using such artificially induced faults might fail in real-world implementations.

This paper is organized as follows: common mode current modeling is presented in Section 2; Section 3 describes test-bench and experiments; common mode current measurement is addressed in Section 4; motor degradation is discussed in Section 5; signal processing and results are presented in Section 6; finally, conclusions are summarized in Section 7.

## 2. Common Mode Current Modeling

Two main approaches have been proposed in the literature for the use of the common mode current for stator winding insulation assessment. The first requires a finite resistance between winding and magnetic core; the second is based on the analysis of HF common mode current resulting from the voltage pulses applied by the inverter. Both are discussed, with the second being the approach used in this paper.

### 2.1. Modeling Using an Equivalent RC Circuit

For ground-wall insulation, the model in Figure 1a has been widely used [2,3,7,10,20–24,29]. The *Dissipation Factor (DF)* or alternatively the *Power Factor (PF)* can be used (1). These methods are especially indicated for machines with voltage ratings of 6 kV and higher [21,22].

$$DF = \tan(\delta) = \frac{|I_r|}{|I_c|} ; \quad PF = \cos(90 - \delta) = \frac{|I_r|}{|I_0|} \quad (1)$$

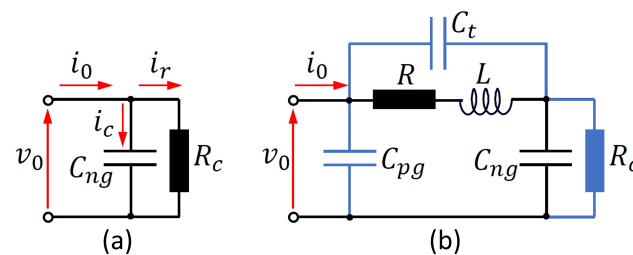


**Figure 1.** Equivalent circuits: (a) RC used mainly for ground-wall insulation analysis; (b) RLC used for HF response analysis. Components in blue can exist or not, depending on the approach.

Detection of ground-wall insulation faults of inverter-fed machines has been reported too. However, in the experiments provided in most of these works, the fault was induced artificially. Capacitors [7] or resistors [2,10,24] were inserted between the neutral of the machine and ground (frame). Capacitors connected to winding taps were used in [6,30] to emulate changes in the inter-turn capacitance, but noting that in these works the phase current transients instead of common mode current were analyzed. In all the cases, the test machine voltage was in the range of hundreds of volts.

A concern for these reports is to what extent conclusions obtained from the analysis of faults induced artificially can be extended to the real faults. A further concern is the sensitivity required by the current sensors used to measure the leakage current in low-voltage machines [7,20,29,30].

## 2.2. Common Mode Voltage Excitation

Common mode voltage pulses applied by the inverter provide a useful form of *HF* excitation for methods using the *HF* components of the common mode current. The common mode voltage applied by the inverter is defined as (2).

$$v_0 = \frac{v_a + v_b + v_c}{3} \quad (2)$$

The output voltage of a two-level inverter can take only two possible values with respect to the midpoint of the inverter:  $-V_{dc}/2$  and  $V_{dc}/2$ . It is deduced from (2) that  $v_0$  can take four possible values,  $v_0 = \{-V_{dc}/2, -V_{dc}/6, V_{dc}/6, V_{dc}/2\}$ . Use of (2) is simplified if the phase voltage commands are zero (3), as in this case all phases will switch simultaneously.

$$v_a^* = v_b^* = v_c^* = 0 ; v_a = v_b = v_c = v_0 \quad (3)$$

For inverters using *PWM/SVM*, the three-phase voltages and the common mode voltage will be a square wave signal (50% duty) varying between  $-V_{dc}/2$  and  $+V_{dc}/2$  in this case [see voltage wave shape in Section 3 Figure 5a] at the switching frequency of the inverter. All the results shown in this paper will be obtained with this type of voltage excitation. One possible disadvantage of this approach is that the method could not be considered *online*, as it is unusual that the inverter operates with zero voltage command. However, this is not considered a drawback. On one hand, the type of fault being detected develops very slowly, with continuous monitoring not being required. In addition, operating with a voltage command equal to zero is easy to achieve after the turn-on of the drive. Furthermore, in this case, the machine would be at (or close to) ambient temperature, mitigating the influence of temperature discussed later.

## 2.3. Modeling Using an Equivalent Resonant Circuit

The use of the *HF* components of the common mode current for diagnostic purposes has been analyzed in [8,25–28]. Modeling of the oscillations of the common mode current using equivalent circuits with passive elements requires the presence of a resonant *LC* network. Several models of this type have been proposed in the literature. The simplest circuit consists of an *RLC* network [28]. This would correspond to the circuit in black in Figure 1b (i.e.,  $C_t = C_{pg} = 0$  and  $R_c = \infty$ ). The corresponding transfer function is (4) in this case.

$$\frac{I_0}{V_0} = \frac{C_{ng}S}{LC_{ng}S^2 + RC_{ng}S + 1} \quad (4)$$

The ground-wall resistance  $R_c$  can be included in the model, the resulting transfer function being (5).

$$\frac{I_0}{V_0} = \frac{C_{ng}R_cS + 1}{LC_{ng}R_cS^2 + (L + C_{ng}RR_c)S + (R + R_c)} \quad (5)$$

This model has been used in [27], and with a slightly different arrangement in [25,26,31]. It is noted that [26,27,31] used distributed parameters, while in [25], lumped parameters are used. In all the experiments performed during this research, it was not possible to detect any *dc* zero currents between windings and magnetic core. However, the sensors and acquisition being used were not specific for the detection of small leakage currents (see Section 4); also, the voltage being applied was relatively small (hundred volts). Consequently, for the analysis presented in this paper, the model in (5) would not add any benefits compared to (4). However, the fact that it includes a zero was found useful for the identification-based analysis presented in Section 6.1.

The model in Figure 1b including capacitors  $C_t$  and  $C_{ng}$  has been used in [8,32]. It is noted that [8,32] used distributed parameters. The fact that the common mode current can flow through a purely capacitive path results in an improper transfer function, i.e., with more zeros than poles. Therefore, model identification discussed in Section 6.1 cannot be applied in this case. Consequently, this model will not be considered. Further discussion on the use of the models presented in this section for insulation assessment is presented in Section 6.1.

### 3. Test Bench and Experiments Description

One objective for the research presented in this paper was that insulation degradation followed a similar process to that occurring in real-world conditions. The use of thermal chambers to achieve accelerated aging has been reported [9,27,29,33]. In [29], the recommendations from IEEE Std 117-2015 [34] were followed. The test conditions applied to Class F motors in [27] were significantly more aggressive than those recommended in [34]. Maximum temperatures of 200 °C and 230 °C are reported in [9,33], respectively, but details on the exposure times are not provided.

Regardless of the benefits of using a thermal chamber, drawbacks must also be considered. Feeding motors operated in a thermal chamber can be extremely challenging. In addition, the thermal chamber results in temperature distribution within the motor, which can be rather different from the temperature distribution in real operating conditions. Although a climatic chamber is available for motor testing, its use was disregarded.

#### 3.1. Test Machine and Three-Phase Inverter

The main test bench consists of two identical induction machines, denoted as *Device Under Test (DUT)* and *Auxiliary (AUX)* motors (see Figures 2 and 3). Main motor parameters are shown in Figure 3. Further details can be found in Section 5. The *DUT* fan was removed; consequently, it reached higher temperatures than *AUX*. Both motors are fed by two three-phase inverters connected back-to-back (see Figures 2 and 3), equipped with 600 V IGBTs. The *dc*-link voltage was limited to 400 V. Phase currents and voltages of both machines were measured using Hall-effect current and voltage sensors of 100 kHz bandwidth. Signals from these sensors were sampled and 750 kHz with 16-bit resolution. A 1024-line encoder is used to measure the speed. Five type-K thermocouple temperature sensors were installed: two inserted into the end-windings of *DUT* motor (see Section 4), two attached to *DUT* and *AUX* frames, and one for ambient temperature. Temperatures were sampled at 1 Hz. For some of the initial experiments, temperature sensors were not operational (0 °C in Figure 7).

The common mode current resonance frequency was found to occur at  $\approx 3$  MHz. Consequently, the current sensor bandwidths and sampling frequencies described above are inadequate to capture this signal. A second concern with the three-phase inverter was that maximum *dc* link voltage was limited to 400 V. Higher voltages are desirable to evaluate the influence of the *dc* voltage on the *HF* common mode current. To overcome these limitations, a *Full-Bridge (FB)* and dedicated sensorization were developed, they are described in Sections 3.2 and 4, respectively.

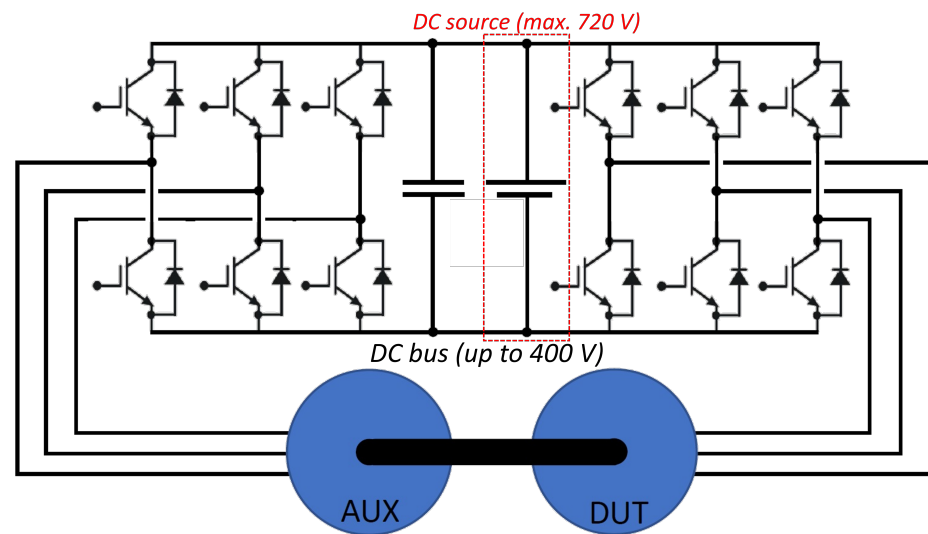


**Figure 2.** Schematic representation of the experimental test bench using two back-to-back inverters.

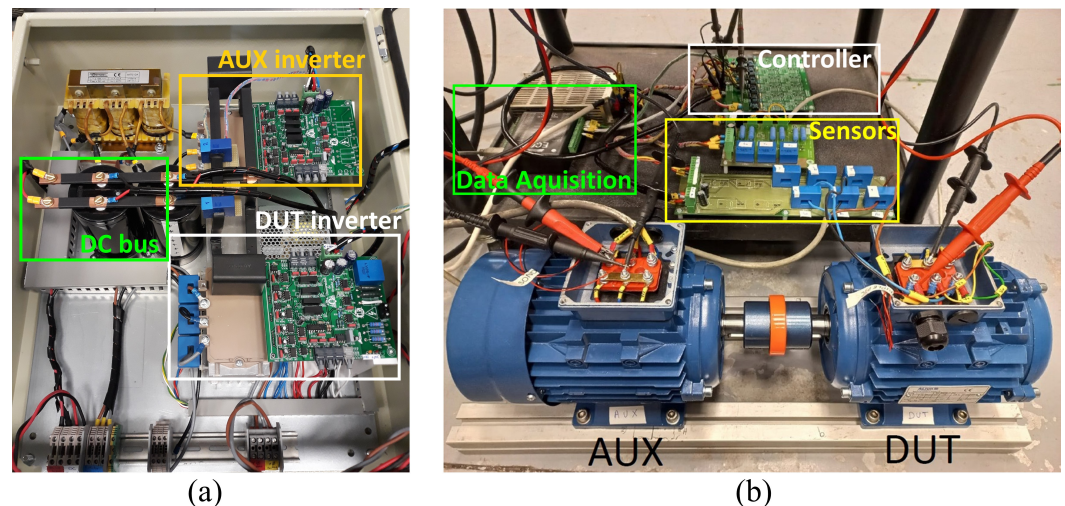


**Figure 3.** Test bench pictures: (a) back-to-back inverters and, (b) DUT and AUX motors. Rated values:  $V = 440 \text{ V}$ ;  $I = 2.74 \text{ A}$ ;  $P = 1.1 \text{ kW}$ ;  $f = 50 \text{ Hz}$ ;  $\omega_r = 1390 \text{ rpm}$ ; 4 poles .

### 3.2. Full-Bridge Converter

The schematic representation of the *FB* converter and *HF* sensorization developed to capture the *HF* common mode current is shown in Figure 4. The *FB* converter uses  $1.2 \text{ kV SiC MOSFET}$ , with a *dc-link* voltage up to  $720 \text{ V}$ . The voltage applied by the *FB* is the same as when the three-phase inverter is commanded zero voltage (3). However, *SiC MOSFET* produces faster commutations than *Si IGBTs*. Furthermore, a voltage step up to  $1440 \text{ V}$  is now possible, compared to the voltage step of  $400 \text{ V}$  achievable with the three-phase inverter.

Figure 5a,b show the voltage pulses applied by the *FB* and the resulting common mode current. Figure 5c,d show the same signals using a zoomed timescale. A conclusion from Figure 5c,d is that the magnitude of the voltage pulses has no visible effects on the common mode current transient. However, when the insulation fault developed, the magnitude of the voltage clearly affected the speed of degradation. This will be discussed later.

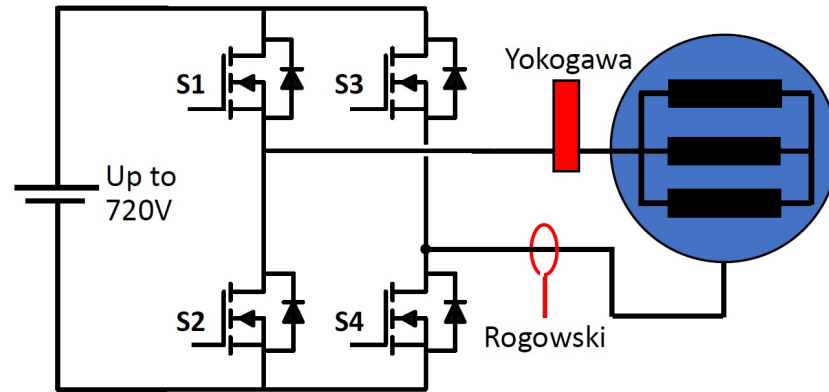


**Figure 4.** Full-bridge and current sensors used to measure the common mode current.

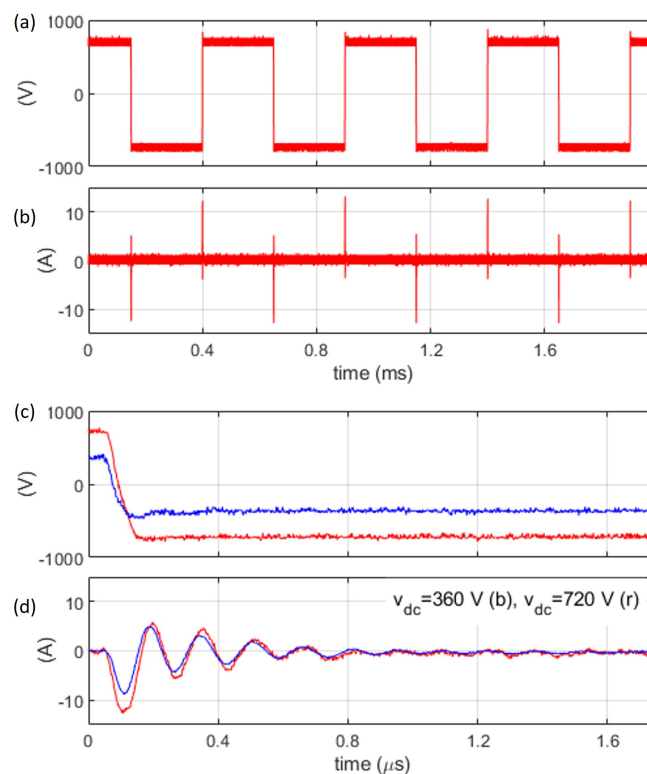


**Figure 5.** (a) Common mode voltage; (b) common mode current. FB switches at 2 kHz,  $v_{dc} = 720$  V; (c,d) zoomed signals for the case of  $v_{dc} = 720$  V (red) and  $v_{dc} = 360$  V (blue), respectively.

### 3.3. Experiment Description

Experiments were performed at a maximum rate of one per day, always starting with the motors at ambient temperature. The *DUT* temperature increase is due exclusively to losses induced during its operation. To accelerate degradation, in some of the experiments *DUT* was forced to operate at temperatures above its class for small periods of time. As mentioned, *DUT* fan was removed. Consequently, *AUX* temperature is significantly lower, its insulation not being jeopardized.

Motors are fed using the back-to-back inverters in Figure 2. Phase currents, voltages, speed, and temperatures are measured and stored. The operating conditions of the motors (control and modulation strategy of inverter feeding *DUT* machine, speed, and torque) vary from experiment to experiment, not being relevant to the contents of this paper. Most of the time the machines operate at rated load as this produces higher losses.

The number of experiments before failure was 28. Figure 6 shows temperatures vs. time for two of them. Both took  $\approx 110$  min, with a maximum *DUT* stator winding

temperature of  $\approx 110$  °C and  $\approx 160$  °C, respectively. Figure 7 shows the duration and maximum temperature for all the experiments carried out. Further discussion on Figure 7 is presented in Section 5.

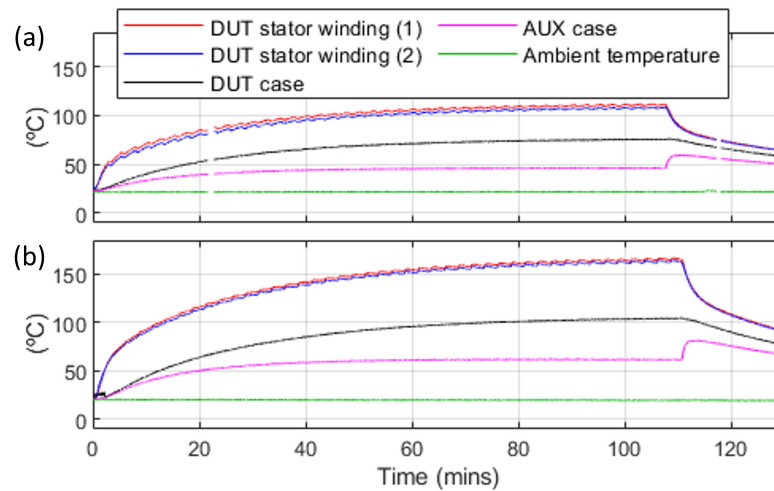


**Figure 6.** Temperatures for experiments (a) #27 and (b) #20 (see Figure 7).

*DUT* phase-to-phase and phase-to-frame insulation was measured using an insulation tester immediately before and after each experiment. The *HF* common mode current measurement using the *FB* was not performed for all the experiments, as disconnection/reconnection of power converters was impractical. However, it was measured before starting any new experiment once phase-to-phase insulation degradation was detected for the first time with the insulation tester (experiment #24 in Figure 7).

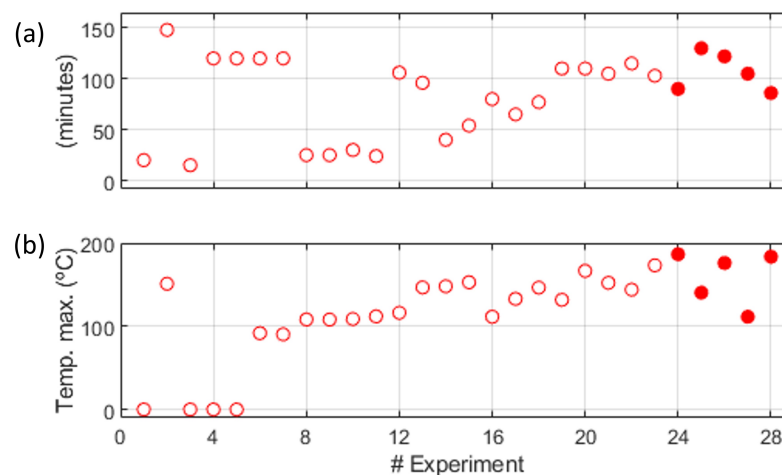


**Figure 7.** Summary of experiments: (a) length in minutes; (b) maximum temperature. Experiments marked with a solid dot indicate that a decrease in phase-to-phase insulation had been detected with the insulation tester.

#### 4. Common Mode Current Measurement

A variety of sensors have been reported in the literature for common mode current analysis. The use of impedance analyzers with embedded sensors is reported in [25,28]; high sensitivity 2 MHz bandwidth differential current transformers were used in [3,20], but noting that in this case, the objective was to detect the leakage current through the winding-to-magnetic core resistance; shunt resistors were mentioned in [27]; use of Rogowski coils is reported in [35,36]; in [35] a 2 MHz magnetoresistive sensor was used; [7,8,29] used a 1 MHz bandwidth current transformer; a current transformer was also used in [26], but the bandwidth was not specified.

From the observed properties for the common mode current, it is concluded that bandwidths in the range of MHz are required. Two current sensors were evaluated: (1) High bandwidth, Hall-effect type instrumentation probe, and (2) Rogowski coil (See Figure 8). For signal acquisition, a conventional digital scope was used. Sensors configuration and connection are shown in Figures 4 and 8a. Measured signals are shown in Figure 9a. Both provide similar responses, the differences could come from the fact that one sensor was located at the cable feeding the stator and the other at the return cable.

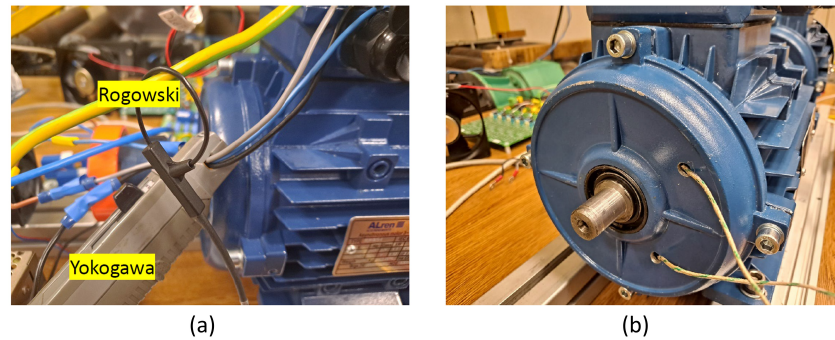


**Figure 8.** (a) Yokogawa Hall-effect and PEM Rogowski sensors. Both provide 50 MHz bandwidth and a maximum current of 30 A; (b) end-frame with the cables connected to two temperature sensors. Temperature sensors are attached to the end coils.

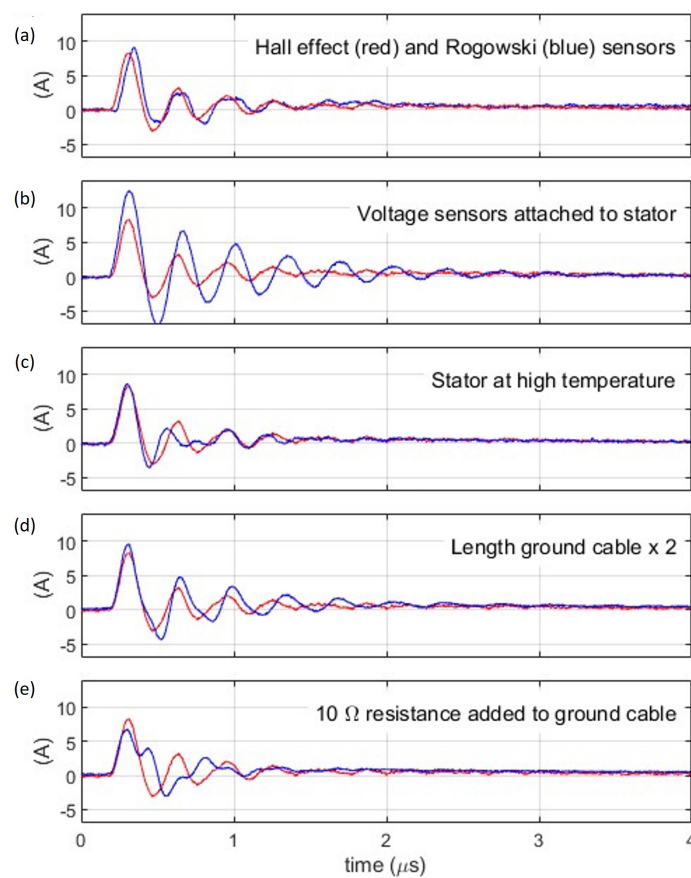


**Figure 9.** Measured common mode current: (a) Hall sensor vs. Rogowski coil at ambient temperature; (b) effect of a voltage sensor attached to the stator; (c) effect due to temperature; (d) effect due to ground cable length; (e) effect due to ground cable resistance.  $V_{dc} = 360$  V. Hall sensor was used for cases (b–e). The trace in red in (a) is shown in all the subplots for reference.



For a real implementation, there are two relevant aspects to consider. First, whether the sensor would be installed permanently, or only when a measurement is to be taken; second, the accuracy required both for sensors and associated electronics to achieve reliable measurements. Considering that the faults being tracked develop slowly and the sensors can be relatively expensive, having the sensors permanently installed might seem an inefficient solution. However, installing the sensor when a measurement is to be taken will give rise to additional concerns, e.g., if the sensor changes from measurement to measurement, or tolerances mounting the sensor. Having the sensor permanently installed would significantly reduce these concerns. In this case, sensor repetitiveness rather than sensor accuracy would be the parameter to consider. On the other hand, *Analog-to-Digital Converters (ADC)* with sampling rates in the range of at least tens of MHz would be required to sample the *HF* common mode current. *ADCs* providing such sampling rates with 16-bit resolution can be found at a reasonable cost. Having them permanently installed might not be therefore prohibitive in some applications.

If the sensor is to be installed only when a measurement is required, the use of open-core sensors would be advantageous. Consequently, the Rogowski coil seems a good option in this case, as it is a flexible, clip-around sensor. Since the information of interest is at *HF*, and in principle the low-frequency components of the common mode currents do not contain useful information, the use of a Rogowski coil without an integrator at its output might be viable [36]. It is noted, however, that this option has not been evaluated experimentally. Sensitivity of Rogowski coil to environmental conditions should also be considered [37].

#### *HF Common Mode Current Sensitivity Analysis*

A number of experiments were performed to understand the sensitivity of the *HF* common mode current to operating and implementation issues. The results are shown in Figure 9b–f. All the measurements were made using the Hall effect sensor. The trace in red in Figure 9a is shown in all the cases for reference. The remaining subplots in Figure 9 show the effect of: (b) connecting Hall-effect type voltage sensors to the stator; (c) increasing the stator temperature; (d) increasing the ground cable length  $\times 2$ ; (e) adding a resistor to the ground cable.

It is concluded from inspection of Figure 9 that the *HF* common mode current is sensitive to changes in the machine temperature, cable impedance, as well as to other elements that could be connected to the stator as voltage sensors. Consequently, to increase the reliability of the measurements, special attention should be paid to minimizing the changes of these parameters during measurements.

### **5. Motor Degradation and Post-Fault Analysis**

The insulation level was measured before and after each experiment using an insulation tester. Phase-to-phase insulation and phase-to-frame insulation for experiments #1 to #23 was  $>10\text{ G}\Omega$ , which was the limit value of the insulation tester. *U – W* insulation decreased to be in the range between  $<10\text{ G}\Omega$  and  $>5\text{ G}\Omega$  after experiment #24. *U – W* failure occurred during common mode current measurement following experiment #28. After this experiment, noise due to partial discharges was readily audible when a common mode voltage of 720 V was applied. Initially, the noise disappeared when the common mode voltage was 360 V. However, the fault evolved very quickly resulting in a net insulation failure between phase *U – W*. No ground-wall fault was detected. Phase *V* remained healthy as well. *DUT* motor was open after failure, with no deterioration in the stator winding being visible.

Insulation fault occurred between phases *U* and *W*. As the stator winding has a single layer with one phase per slot, the fault necessarily occurred in the end-winding. End-windings have been reported to be the hottest spot in electric machines [38]. Figure 10 shows the measured resistance between phases *U* and *W* using the four possible combinations and the estimated location of the fault. The phase resistances and phase-to-frame capacitance

for the healthy case and after the last test are shown in Table 1. Capacitance for phase *U* and *W* after the fault is the same as they are short-circuited. Resistance and capacitance for the healthy phase increased slightly.

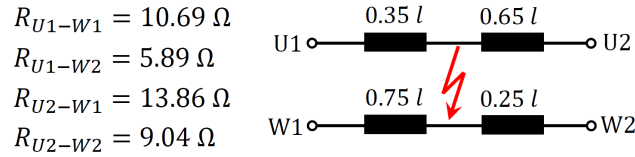


**Figure 10.** Measured resistances and estimated location of the fault between phases *U* and *W* in p.u. of winding length *l*.

**Table 1.** *DUT* *dc* stator resistance and capacitance.

	Healthy	Faulty		Healthy	Faulty
$R_{U1-U2}$	9.67 $\Omega$	9.8 $\Omega$	$C_{U-g}$	0.852 nF	1.43 nF
$R_{V1-V2}$	9.55 $\Omega$	9.75 $\Omega$	$C_{V-g}$	0.888 nF	0.977 nF
$R_{W1-W2}$	9.7 $\Omega$	9.9 $\Omega$	$C_{W-g}$	0.959 nF	1.43 nF

Figure 11 shows captures with the thermal imaging camera when a *dc* voltage is applied to the stator terminals indicated in the corresponding captions. The voltage was adjusted manually to obtain the nominal current. The images confirm that the insulation fault occurred in the end-winding, and not in the cables connecting the terminal box to the winding.

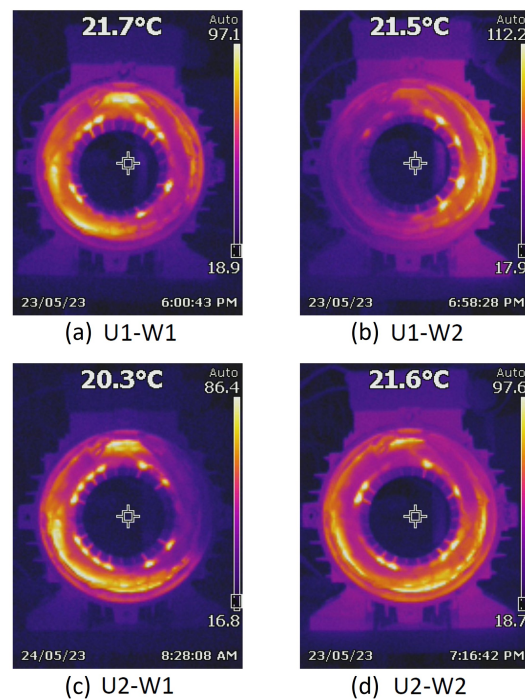


**Figure 11.** Captures of the thermal imaging camera after test #28 when the stator is fed from a *dc* voltage source between terminals indicated in the subcaptions. The stator has 24 slots, single-layer winding.

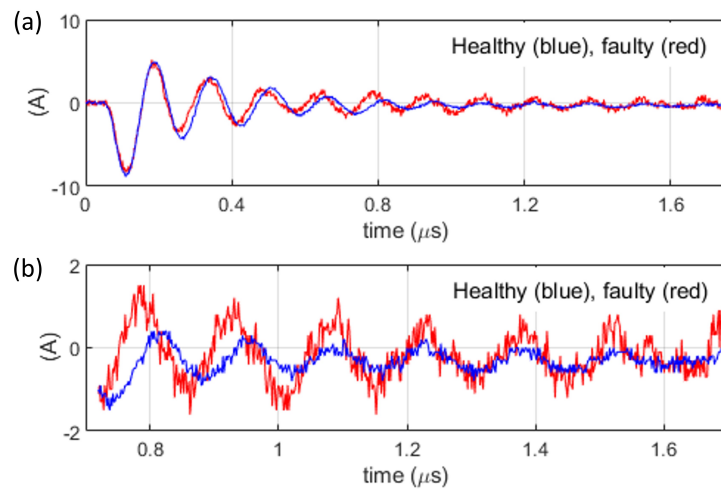
## 6. HF Common Mode Current Analysis and Processing

Figure 12a shows the common mode current for the case of a healthy machine, and for the case when an insulation decrease was detected for the first time with the insulation

tester (experiment #24, see Figure 7). It is noted that although the figure shows a single pulse, the response is highly repetitive.

At first glance, the response for both cases looks very similar. A closer look reveals that the coincidence is most remarkable during the initial part of the transient. Figure 12b shows the common mode current after removing the initial part of the transient in Figure 12a. This signal is denoted as  $i_{0W}$ . It is observed that the oscillations of *DUT* once insulation degradation has started last longer (lower damping). Interestingly, this change in behavior of the common mode current remained almost unaltered for all the measurements of the common mode current performed previous to the start of experiments #25 to #28 in Figure 7. Furthermore, the behavior persisted even when the machine could not be fed from the inverter due to the lack of insulation between phases.

Different forms of signal processing of the common mode current are discussed in the following subsections.



**Figure 12.** (a) Transient common mode current for the healthy and faulty cases. (b) Windowed common mode current  $i_{0W}$ ; obtained by applying a window  $W$  to  $i_0$ .  $W = 1$  for  $0.75 \mu\text{s} < t < 1.7 \mu\text{s}$ ;  $W = 0$  otherwise.

### 6.1. Insulation Assessment Based on Model Estimation

The peak value of the common mode current was used in [26,27] as a possible indicator of the insulation condition. However, from the results obtained in this work, the peak value alone was not found to be a reliable metric. The common mode voltage-to-current frequency response function was used in [8,25,32]. Changes either in the peak value or in the frequency response function would be connected with system pole migration in (4), (5) due to changes in machine parameters. It would, therefore, be expected that the migration of model parameters could provide useful information on the insulation condition.

Model identification using the measured common mode current was implemented using Matlab. The function `procest` with a model structure of two underdamped poles and a zero provided the best fit to estimation data, the system resulting from the identification being of the form (6).

$$\frac{I_0}{V_0} = k \frac{(\tau_z s + 1)}{(\tau_w s)^2 + 2\zeta\tau_w s + 1} \tag{6}$$

Under the assumption that  $R_c \gg R$ , the following relationship can be found between (6) and (5).

$$\tau_w \approx \sqrt{LC_{ng}}; \zeta \approx \frac{R}{2} \sqrt{\frac{C_{ng}}{L}}; \tau_z = C_{ng}R_c; k = \frac{1}{L} \tag{7}$$

To reduce the sensitivity to noise or other possible disturbances, parameter identification was performed by averaging the common mode current resulting in eight successive common mode voltage transitions, as shown in Figure 5.

To validate the estimated model, its response was obtained using Matlab function `lsim`, with the input being the measured voltage. Figure 13 shows the actual and simulated common mode current. A good agreement is observed in general.

Table 2 shows the result obtained averaging the eight estimations,  $\omega_d = \omega_n \sqrt{1 - \zeta^2}$  being the damped natural frequency. A difference between the healthy and faulty cases in Figure 12 is the reduction in the estimated damping for the case of the faulty machine (oscillations last longer). This is consistent with the behavior of the damping factor  $\zeta$  observed in Table 2. It is deduced from (7) that a decrease in  $\zeta$  can be due to a decrease in either  $R$  and/or  $C_{ng}$ , or to an increase on  $L$ . Unfortunately, the decrease observed is in the range of 5% to 10%, which might not be enough for reliable detection. A second difference observed in Figure 12 between the healthy and the faulty cases is an increase in the damped natural frequency  $\omega_d$ . However, this is not confirmed by the results in Table 2, as the trend observed for the cases 360 V and 720 V are opposite.

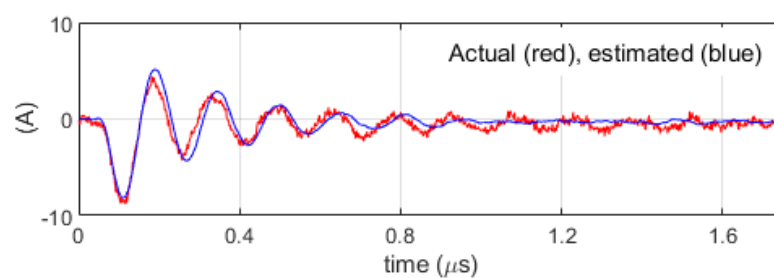


Figure 13. Actual and estimated common mode current using the parametric model in (6).

Table 2. Model identification: Experimental results.

DUT	Voltage (V)	$\omega_d$ (Hz)	$\zeta$	$1/\tau_z$ (Hz)	$k$
Healthy	360	6,749,592	0.1167	6,820,495	380
Faulty	360	70,073,690	0.1042	7,089,280	340
Healthy	720	7,216,209	0.1103	7,261,304	417
Faulty	720	6,888,639	0.1049	6,941,588	359

## 6.2. Insulation Assessment Based on Frequency Analysis

It was already shown in Figure 12 that a remarkable difference between the healthy and faulty cases was the persistence of the oscillations for the second case. This suggests the use of frequency-based methods. For this purpose, it is advantageous to remove the initial part of the common mode current transient due to two reasons: first, no relevant differences are observed between the healthy and faulty cases during the initial part of the transient; second, frequency-based methods are not effective in analyzing transient phenomena. A similar approach to the one described following was proposed in [35].

Figure 14 shows the *FFT* of the common mode current after removing the initial part of the transient (see Figure 12b). It is noted that with the time window used in Figure 12b, the oscillation occurs at the 7th harmonic. The increase in the peak values between the faulty and healthy cases observed in Figure 14 is seen in all cases in the range of 220%, and can be considered therefore significantly more reliable than the changes in  $\zeta$  observed in Section 6.1.

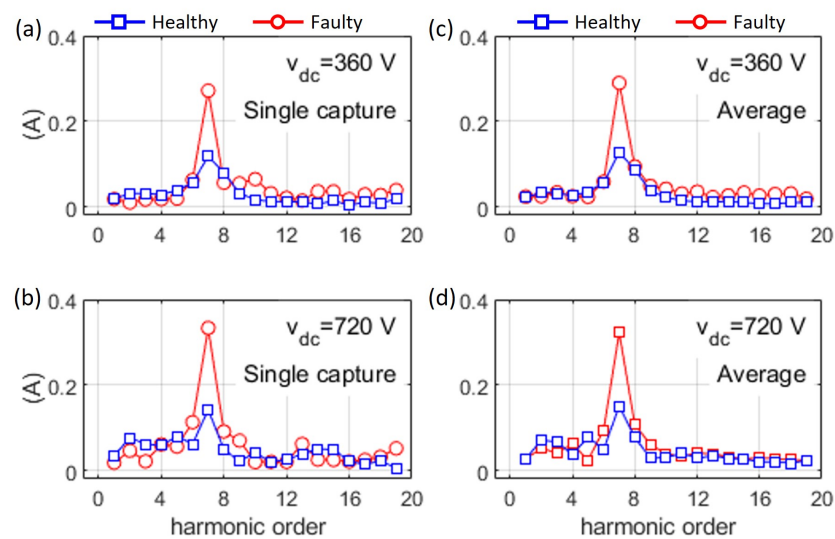


**Figure 14.**  $|FFT(i_{0W})|$  [see Figure 12b]. Left (a,b): single capture, right (c,d): average of eight successive captures. Top (a,c):  $V_{dc} = 360$  V, bottom (b,d):  $V_{dc} = 720$  V. Blue/Red: healthy/faulty machine.

Regardless of the promising results, there are a few aspects to consider for the described signal processing. First, it is based on the assumption that the frequency of the oscillation does not change significantly between the healthy and faulty cases. Also, the length of the initial transient being removed, as well as the length of the common mode current window being processed, were adjusted manually. It would be desirable to automatize this process. For example, *PLL* could be used to estimate the frequency of the oscillation and adapt the *FFT*. However, more experimental data is needed to solve these uncertainties.

### 6.3. Other Forms of Signal Processing

The dependency on the oscillation frequency discussed in the previous section could be avoided if instead of focusing on a single component of the spectrum, the total energy of the common mode current is considered. The *RMS* value of the common mode current can be used for this purpose. Table 3 summarizes the results obtained using this approach. It is observed that if the initial part of the transient is not removed,  $RMS(i_0)$  actually decreases for the faulty case with respect to the healthy case. This is due to the fact that most of the energy of the signal occurs on the initial part of the transient, which is not affected by insulation deterioration. This problem is solved by using  $RMS(i_{0W})$ . However, significant differences are observed for the case of  $V_{dc} = 360$  and 720 V. Also, the sensitivity is significantly smaller compared to using the *FFT*.

**Table 3.**  $RMS(i_0)$ .

<i>DUT</i>	Voltage (V)	$i_0$ (A)	$i_{0W}$ (A)	Voltage (V)	$i_0$ (A)	$i_{0W}$ (A)
Healthy	360	1.807	0.436	720	2.67	0.792
Faulty	360	1.737	0.644	720	2.4722	0.897
$\Delta(i_0)\%$	360	−4%	47%	720	−7%	13%

It is finally noted that many other forms of signal processing, e.g., based on correlations or wavelet-based analysis [39], could be used. Independent of the approach being used, it is concluded from the results presented in this work that a single measurement of the *HF* common mode current is not enough to determine the insulation condition of a machine. Tracking the deviations with respect to when the machine was healthy is required. It is noted that the same applies to other methods for insulation degradation detection [21,22].

## 7. Conclusions

A case study of stator windings insulation condition assessment for inverter-fed machines using the *HF* common mode current has been presented in this paper. Implementation of the proposed method requires the use of a high bandwidth current sensor and acquisition system. The cost of these elements can be relevant for low-power, cheap induction motor drives. However, it could be fully justified in high-power (hundred kW), high efficiency, expensive induction motor drives, e.g., for railway traction. Implementation of the method does not require changes in the system layout and does not interfere with drive normal operation either. These elements could be installed permanently or only when a measurement is to be taken, both options having pros and cons.

Aging was accelerated by performing a sequence of experiments in which the machine was forced to operate at temperatures above its class. Phase-to-phase insulation failure finally occurred in the end-winding. Visual inspection did not reveal any anomaly.

Two main types of signal processing methods were used: model-based and *FFT*-based, with the second showing a significantly better detection capability when applied to the windowed common mode current. As the behavior of the common mode current is specific to each machine design, the signal processing should be tuned accordingly.

The sensitivity of the *HF* common mode current to operating conditions and system configuration was also evaluated. Winding temperatures can have significant effects. Consequently, measurements should be carried out with the machine at a similar temperature. Realizing the measurements at the start-up of the drive seems to be the most reliable option.

From the results shown in this paper, it is concluded that a single measurement of the *HF* common mode current is not enough to determine the insulation condition, trends over time should be tracked. It is noted that the same concern applies to other methods as *DF* and *PF*.

A limitation of the results presented in this paper is that the analysis was limited to a specific fault. However, this fault resulted from operating the machine repeatedly under extreme working conditions; no external elements were added. Consequently, the results shown are believed to be a true subset of the phenomena that could happen in practice.

**Author Contributions:** Conceptualization, M.S. and F.B.; methodology, M.S., J.M.G. and F.B.; software, M.S., J.M.G. and D.F.; validation, F.B., I.D. and M.S.; formal analysis, J.M.G. and F.B.; investigation, M.S. and J.M.G.; resources, F.B. and J.M.G.; data curation, F.B. and I.D.; writing—original draft preparation, F.B. and M.S.; writing—review and editing, J.M.G., I.D. and D.F.; visualization, M.S. and F.B.; supervision, F.B.; project administration, F.B.; funding acquisition, F.B. and J.M.G. All authors have read and agreed to the published version of the manuscript.

**Funding:** This work was supported in part by Ingeteam Power Technology S.A. and by the Government of the Principality of Asturias under project AYUD/2021/50988.

**Data Availability Statement:** Data are contained within the article.

**Conflicts of Interest:** The authors declare no conflicts of interest.

## Abbreviations

The following abbreviations are used in this manuscript:

<i>MCSA</i>	Motor Current Signature Analysis
<i>HF</i>	High Frequency
<i>DUT</i>	Device Under Test
<i>AUX</i>	Auxiliary
<i>FB</i>	Full-Bridge
<i>ADC</i>	Analog-to-Digital Converters
<i>DF</i>	Dissipation Factor
<i>PF</i>	Power Factor

## References

1. Surya, G.N.; Khan, Z.J.; Ballal, M.S.; Suryawanshi, H.M. A Simplified Frequency-Domain Detection of Stator Turn Fault in Squirrel-Cage Induction Motors Using an Observer Coil Technique. *IEEE Trans. Ind. Electron.* **2017**, *64*, 1495–1506. [[CrossRef](#)]
2. Lee, S.B.; Younsi, K.; Kliman, G. An online technique for monitoring the insulation condition of AC machine stator windings. *IEEE Trans. Energy Convers.* **2005**, *20*, 737–745. [[CrossRef](#)]
3. Zhang, P.; Younsi, K.; Neti, P. A Novel Online Stator Ground-Wall Insulation Monitoring Scheme for Inverter-Fed AC Motors. *IEEE Trans. Ind. Appl.* **2015**, *51*, 2201–2207. [[CrossRef](#)]
4. Stone, G.; Campbell, S.; Tetreault, S. Inverter-fed drives: Which motor stators are at risk? *IEEE Ind. Appl. Mag.* **2000**, *6*, 17–22. [[CrossRef](#)]
5. Xu, Y.; Yuan, X.; Ye, F.; Wang, Z.; Zhang, Y.; Diab, M.; Zhou, W. Impact of High Switching Speed and High Switching Frequency of Wide-Bandgap Motor Drives on Electric Machines. *IEEE Access* **2021**, *9*, 82866–82880. [[CrossRef](#)]
6. Zoeller, C.; Vogelsberger, M.A.; Wolbank, T.M.; Ertl, H. Impact of SiC semiconductors switching transition speed on insulation health state monitoring of traction machines. *IET Power Electron.* **2016**, *9*, 2769–2775. [[CrossRef](#)]
7. Zheng, D.; Zhang, P. An Online Groundwall and Phase-to-Phase Stator Insulation Monitoring Method for Inverter-Fed Machine. *IEEE Trans. Ind. Electron.* **2021**, *68*, 5303–5313. [[CrossRef](#)]
8. Zheng, D.; Lu, G.; Zhang, P. An Improved Online Stator Insulation Monitoring Method Based on Common-Mode Impedance Spectrum Considering the Effect of Aging Position. *IEEE Trans. Ind. Appl.* **2022**, *58*, 3558–3566. [[CrossRef](#)]
9. Alvarez-Gonzalez, F.; Hewitt, D.; Griffio, A.; Wang, J.; Diab, M.; Yuan, X. Design of Experiments for Stator Windings Insulation Degradation under High  $dv/dt$  and High Switching Frequency. In Proceedings of the IEEE Energy Conversion Congress and Exposition (ECCE), Detroit, MI, USA, 11–15 October 2020; pp. 789–795. [[CrossRef](#)]
10. Lee, S.B.; Yang, J.; Younsi, K.; Bharadwaj, R. An online groundwall and phase-to-phase insulation quality assessment technique for AC-machine stator windings. *IEEE Trans. Ind. Appl.* **2006**, *42*, 946–957. [[CrossRef](#)]
11. Cruz, J.d.S.; Fruett, F.; Lopes, R.d.R.; Takaki, F.L.; Tambascia, C.d.A.; Lima, E.R.d.; Giesbrecht, M. Partial Discharges Monitoring for Electric Machines Diagnosis: A Review. *Energies* **2022**, *15*, 7966. [[CrossRef](#)]
12. Jung, J.H.; Lee, J.J.; Kwon, B.H. Online Diagnosis of Induction Motors Using MCSA. *IEEE Trans. Ind. Electron.* **2006**, *53*, 1842–1852. [[CrossRef](#)]
13. Afrandideh, S.; Haghjoo, F.; Cruz, S.; Eshaghi Milasi, M. Detection of Turn-to-Turn Faults in the Stator and Rotor of Synchronous Machines During Startup. *IEEE Trans. Ind. Electron.* **2021**, *68*, 7485–7495. [[CrossRef](#)]
14. Gandhi, A.; Corrigan, T.; Parsa, L. Recent Advances in Modeling and Online Detection of Stator Interturn Faults in Electrical Motors. *IEEE Trans. Ind. Electron.* **2011**, *58*, 1564–1575. [[CrossRef](#)]
15. Briz, F.; Degner, M.W.; Garcia, P.; Diez, A.B. High-Frequency Carrier-Signal Voltage Selection for Stator Winding Fault Diagnosis in Inverter-Fed AC Machines. *IEEE Trans. Ind. Electron.* **2008**, *55*, 4181–4190. [[CrossRef](#)]
16. Pietrzak, P.; Wolkiewicz, M. Comparison of Selected Methods for the Stator Winding Condition Monitoring of a PMSM Using the Stator Phase Currents. *Energies* **2021**, *14*, 1630. [[CrossRef](#)]
17. Wolkiewicz, M.; Tarchała, G.; Orłowska, T.; Kowalski, C.T. Online Stator Interturn Short Circuits Monitoring in the DFOC Induction-Motor Drive. *IEEE Trans. Ind. Electron.* **2016**, *63*, 2517–2528. [[CrossRef](#)]
18. Bazan, G.H.; Scalassara, P.R.; Endo, W.; Goedel, A.; Palácios, R.H.C.; Godoy, W.F. Stator Short-Circuit Diagnosis in Induction Motors Using Mutual Information and Intelligent Systems. *IEEE Trans. Ind. Electron.* **2019**, *66*, 3237–3246. [[CrossRef](#)]
19. Mazzeletti, M.A.; Bossio, G.R.; De Angelo, C.H.; Espinoza-Trejo, D.R. A Model-Based Strategy for Interturn Short-Circuit Fault Diagnosis in PMSM. *IEEE Trans. Ind. Electron.* **2017**, *64*, 7218–7228. [[CrossRef](#)]
20. Neti, P.; Younsi, K.; Shah, M.R. A novel high sensitivity differential current transformer for online health monitoring of industrial motor ground-wall insulation. In Proceedings of the 2013 IEEE Energy Conversion Congress and Exposition, Denver, CO, USA, 15–19 September 2013; pp. 2493–2499. [[CrossRef](#)]
21. IEC 60034-27-3:2015; Rotating Electrical Machines—Part 27-3: Dielectric Dissipation Factor Measurements on Stator Winding Insulation of Rotating Electrical Machines. IEC Standards: Geneva, Switzerland, 2015; pp. 1–34.
22. IEEE Std 286-2000; IEEE Recommended Practice for Measurement of Power Factor Tip-Up of Electric Machinery Stator Coil Insulation. IEEE Standards Association: Piscataway, NJ, USA, 2000. [[CrossRef](#)]
23. Pascoli, G.; Hribernik, W.; Ujvari, G. A practical investigation on the correlation between aging and the dissipation factor value of mica insulated generator windings. In Proceedings of the International Conference on Condition Monitoring and Diagnosis, Beijing, China, 21–24 April 2008; pp. 268–271. [[CrossRef](#)]
24. Yang, J.; Lee, S.B.; Yoo, J.; Lee, S.; Oh, Y.; Choi, C. A Stator Winding Insulation Condition Monitoring Technique for Inverter-Fed Machines. *IEEE Trans. Power Electron.* **2007**, *22*, 2026–2033. [[CrossRef](#)]
25. Neti, P.; Grubic, S. Online Broadband Insulation Spectroscopy of Induction Machines Using Signal Injection. *IEEE Trans. Ind. Appl.* **2017**, *53*, 1054–1062. [[CrossRef](#)]
26. Niu, F.; Wang, Y.; Huang, S.; Wu, L.; Huang, X.; Fang, Y.; Yang, T. An Online Groundwall Insulation Monitoring Method Based on Transient Characteristics of Leakage Current for Inverter-Fed Motors. *IEEE Trans. Power Electron.* **2022**, *37*, 9745–9753. [[CrossRef](#)]
27. Jensen, W.R.; Strangas, E.G.; Foster, S.N. A Method for Online Stator Insulation Prognosis for Inverter-Driven Machines. *IEEE Trans. Ind. Appl.* **2018**, *54*, 5897–5906. [[CrossRef](#)]

28. Cao, S.; Niu, F.; Huang, X.; Huang, S.; Wang, Y.; Li, K.; Fang, Y. Time-Frequency Characteristics Research of Common Mode Current in PWM Motor System. *IEEE Trans. Power Electron.* **2020**, *35*, 1450–1458. [[CrossRef](#)]
29. Tsyokhla, I.; Griffo, A.; Wang, J. Online Condition Monitoring for Diagnosis and Prognosis of Insulation Degradation of Inverter-Fed Machines. *IEEE Trans. Ind. Electron.* **2019**, *66*, 8126–8135. [[CrossRef](#)]
30. Nussbaumer, P.; Vogelsberger, M.A.; Wolbank, T.M. Induction Machine Insulation Health State Monitoring Based on Online Switching Transient Exploitation. *IEEE Trans. Ind. Electron.* **2015**, *62*, 1835–1845. [[CrossRef](#)]
31. Ryu, Y.; Park, B.R.; Han, K.J. Estimation of High-Frequency Parameters of AC Machine From Transmission Line Model. *IEEE Trans. Magn.* **2015**, *51*, 8101404. [[CrossRef](#)]
32. Zheng, D.; Zhang, P. A Novel Method of Monitoring and Locating Stator Winding Insulation Ageing for Inverter-fed Machine based on Switching Harmonics. In Proceedings of the IEEE Energy Conversion Congress and Exposition (ECCE), Detroit, MI, USA, 11–15 October 2020; pp. 4474–4479. [[CrossRef](#)]
33. Bolgova, V.; Lefebvre, S.; Hlioui, S.; Boucenna, N.; Costa, F.; Leonov, A. Development of testing methods for winding turn-to-turn insulation of low voltage motors fed by PWM converters. In Proceedings of the 19th European Conference on Power Electronics and Applications (EPE'17 ECCE Europe), Warsaw, Poland, 11–14 September 2017; pp. 1–10. [[CrossRef](#)]
34. *IEEE Std 117-2015 (Revision of IEEE Std 117-1974)*; IEEE Standard Test Procedure for Thermal Evaluation of Systems of Insulating Materials for Random-Wound AC Electric Machinery. IEEE Standards Association: Piscataway, NJ, USA, 2016; pp. 1–34. [[CrossRef](#)]
35. Zanuso, G.; Peretti, L. Evaluation of High-Frequency Current Ringing Measurements for Insulation Health Monitoring in Electrical Machines. *IEEE Trans. Energy Convers.* **2022**, *37*, 2637–2644. [[CrossRef](#)]
36. Poncelas, O.; Rosero, J.A.; Cusido, J.; Ortega, J.A.; Romeral, L. Motor Fault Detection Using a Rogowski Sensor Without an Integrator. *IEEE Trans. Ind. Electron.* **2009**, *56*, 4062–4070. [[CrossRef](#)]
37. Mingotti, A.; Costa, F.; Peretto, L.; Tinarelli, R. Accuracy Type Test for Rogowski Coils Subjected to Distorted Signals, Temperature, Humidity, and Position Variations. *Sensors* **2022**, *22*, 1397. [[CrossRef](#)]
38. Tovar-Barranco, A.; López-de Heredia, A.; Villar, I.; Briz, F. Modeling of End-Space Convection Heat-Transfer for Internal and External Rotor PMSMs With Fractional-Slot Concentrated Windings. *IEEE Trans. Ind. Electron.* **2021**, *68*, 1928–1937. [[CrossRef](#)]
39. Briz, F.; Degner, M.W.; Garcia, P.; Bragado, D. Broken Rotor Bar Detection in Line-Fed IM Using Complex Wavelet Analysis of Startup Transients. *IEEE Trans. Ind. Appl.* **2008**, *44*, 760–768. [[CrossRef](#)]

**Disclaimer/Publisher’s Note:** The statements, opinions and data contained in all publications are solely those of the individual author(s) and contributor(s) and not of MDPI and/or the editor(s). MDPI and/or the editor(s) disclaim responsibility for any injury to people or property resulting from any ideas, methods, instructions or products referred to in the content.